Interaction of DNA with the Klenow Fragment of DNA Polymerase I Studied by Time-Resolved Fluorescence Spectroscopy†

Christopher R. Guest,‡ Remo A. Hochstrasser,‡ Charles G. Dupuy,‡,∥ Dwayne J. Allen,§,⊥ Stephen J. Benkovic,§ and David P. Millar*,‡

Department of Molecular Biology, Research Institute of Scripps Clinic, 10666 North Torrey Pines Road, La Jolla, California 92037, and Department of Chemistry, The Pennsylvania State University, University Park, Pennsylvania 16802

Received March 20, 1991; Revised Manuscript Received June 17, 1991

ABSTRACT: The interaction of a fluorescent duplex DNA oligomer with the Klenow fragment of DNA polymerase I from *Escherichia coli* has been studied in solution by using time-resolved fluorescence spectroscopy. An aminonaphthalenesulfonate (dansyl) fluorescent probe was linked by a propyl chain to a C5-modified uridine base located at a specific site in the primer strand of the DNA oligomer. The fluorescent oligomer bound tightly to the Klenow fragment (K_D = 7.9 nM), and the probe's position within the DNA–protein complex was varied by stepwise elongation of the primer strand upon addition of the appropriate deoxynucleoside triphosphates. The decay of the total fluorescence intensity and the polarization anisotropy were measured with a picosecond laser and a time-correlated single photon counting system. The fluorescence lifetimes, the correlation time for internal rotation, and the angular range of internal rotation varied according to the probe's position within the DNA–protein complex. These results showed that five or six bases of the primer strand upstream of the 3′ terminus were in contact with the protein and that within this contact region there were differences in the degree of solvent accessibility and the closeness of contact. Further, a minor binding mode of the DNA–protein complex was identified, on the basis of heterogeneity of the probe environment observed when the probe was positioned seven bases upstream from the primer 3′ terminus, which resulted in a distinctive "dip and rise" in the anisotropy decay. Experiments with an epoxy-terminated DNA oligomer and a site-directed mutant protein established that the labeled DNA was binding at the polymerase active site (major form) and at the spatially distinct 3′→5′ exonuclease active site (minor form). The abundance of each of these distinct binding modes of the DNA–protein complex was estimated under solution conditions by analyzing the anisotropy decay of the dansyl probe. About 12% of the labeled DNA was bound at the 3′→5′ exonuclease site. This method should be useful for investigating the editing mechanism of this important enzyme.

DNA polymerase I (Pol I) is a multifunctional enzyme involved in the repair and replication of DNA in *Escherichia coli* (Kornberg, 1980). In addition to a 5′→3′ polymerase activity that catalyzes the template-directed polymerization of deoxynucleoside triphosphates (dNTP's) onto a primer strand, the enzyme also possesses a separate 3′→5′ exonuclease activity capable of removing nucleotides from the primer strand and a 5′→3′ exonuclease activity which removes nucleotides in front of the growing primer strand (Jovin et al., 1969). The fidelity of DNA synthesis catalyzed by Pol I is enhanced by the 3′→5′ exonuclease activity, which edits mismatched nucleotides mistakenly incorporated by the polymerase activity.

The large proteolytic fragment of Pol I, known as the Klenow fragment, retains the polymerase and the 3′→5′ exonuclease activities (Brutlag et al., 1969). The crystal structure of the Klenow fragment has been solved at 3.3-Å resolution (Ollis et al., 1985) and shows that the polypeptide chain is folded into two domains. The larger C-terminal domain (413 residues) has been overexpressed and purified to yield a protein which exhibits polymerase activity but lacks measurable exonuclease activity (Freemont et al., 1986), thereby suggesting that the active site for the polymerase reaction is contained in the C-terminal domain. The smaller N-terminal domain (182 residues) contains a binding site for deoxynucleoside monophosphates (dNMP's) (Ollis et al., 1985), the product of the exonuclease reaction. Site-directed mutagenesis of residues within the dNMP binding site can eliminate 3′→5′ exonuclease activity without affecting polymerase activity, showing that the 3′→5′ exonuclease active site is contained in the N-terminal domain (Derbyshire et al., 1988).

The C-terminal domain contains a large cleft with dimensions suitable for binding a duplex DNA molecule (Warwicker et al., 1985). However, when a synthetic duplex DNA oligomer was cocrystallized with the Klenow fragment under the low ionic strength conditions in which the enzyme is active, the DNA was not visible in the crystal structure (Joyce & Steitz, 1987; Steitz, 1990), suggesting that this complex of duplex DNA and Klenow fragment was disordered on the time scale of the X-ray diffraction experiment. However, when the crystallization was performed under high salt conditions, a portion of the primer strand of the DNA was visible on the N-terminal domain of the enzyme, suggesting that the 3′→5′ exonuclease site contains a binding site for single-stranded DNA (Freemont et al., 1988).

A model based on chemical footprinting (Joyce & Steitz, 1987) suggests that 8 base pairs of duplex DNA lie within the cleft in the C-terminal domain when the primer 3′ terminus

† Supported by the Research Institute of Scripps Clinic (D.P.M.) and the Swiss National Science Foundation (R.A.H.).

* Author to whom correspondence should be addressed.
‡ Research Institute of Scripps Clinic.
§ The Pennsylvania State University.
∥ Present address: David Sarnoff Research Center, Princeton, NJ 08543.
⊥ Present address: Department of Biochemistry, Duke University Medical Center, Durham, NC 27707.

0006-2960/91/0430-8759$02.50/0

is bound in the active site for the polymerization reaction. However, during editing, the primer 3′ terminus must be bound in the region of the dNMP binding site, which is separated from the putative polymerase active site by about 30 Å (Joyce & Steitz, 1987). This raises the interesting question of how the two active sites work together during DNA synthesis to maintain the high fidelity. Joyce and Steitz (1987) proposed that the protein slides on the DNA over a distance of about 8 base pairs to bring the exonuclease site into proximity with the primer 3′ terminus and that the four 3′-terminal bases of the primer strand melt-out in order to bind to the single-strand DNA binding region on the exonuclease domain. Direct support for the 8 base pair distance between the polymerase and 3′→5′ exonuclease active sites and associated melting of the primer terminus was furnished by fluorescence energy-transfer experiments (Allen & Benkovic, 1989) as well as studies employing biotinylated oligonucleotide duplexes and site-specifically cross-linked DNA (Cowart et al., 1989).

In order to understand the molecular basis of editing by the Klenow fragment and to test the predictions of the model outlined above, we have studied the interaction of a fluorescent duplex DNA oligomer with the Klenow fragment using time-resolved fluorescence spectrosocpy. DNA duplexes of defined sequence that contain an aminonaphthalenesulfonate (dansyl) fluorescent probe linked to a C5-modified uridine nucleotide at a specific site in the primer chain were used as substrates for the Klenow fragment. The fluorescence properties of the aminonaphthalenesulfonates are environmentally sensitive and have previously been used to detect substrate binding to proteins (Ondera et al., 1976). The steady-state emission parameters of the fluorescent duplex have been previously reported (Allen et al., 1989). The emission maximum, emission intensity, and steady-state polarization anisotropy exhibit characteristic changes upon binding of the duplex to the Klenow fragment and upon variation of the probe's position within the DNA–protein complex. In the present study, we have used time-resolved fluorescence spectroscopy to provide a more detailed view of the complex formed between DNA and the Klenow fragment, since the equilibrating distribution of binding modes of the complex will be frozen on the short time scale characteristic of fluorescence lifetimes, and the distinct binding modes can then be identified and their relative abundance can be estimated under solution conditions. The fluorescent probe was positioned within the DNA oligomer such that it was exposed to different local environments when the primer terminus bound to either the polymerase or the 3′→5′ exonuclease active sites of the Klenow fragment. The resulting fluorophore heterogeneity generated a distinctive "dip and rise" in the decay of the fluorescence polarization anisotropy on the nanosecond time scale. The precise form of the decay was demonstrated to be a sensitive function of the relative abundance of the two binding modes of the DNA–protein complex, even though the two modes of the complex are interconverting on slower time scales.

A preliminary account of part of this work has appeared elsewhere (Millar et al., 1990).

Experimental Procedures

Materials. Klenow fragment was purified from *E. coli* strain CJ333 (Joyce et al., 1985) and was at least 99% homogeneous according to polyacrylamide gel electrophoresis. The mutant protein D355A, E357A (Asp-355 → Ala, Glu-357 → Ala) was prepared from a clone kindly furnished by C. Joyce and was purified as described (Derbyshire et al., 1988). The proteins were stored at −70 °C in a buffer of 50 mM Tris-HCl, pH 7.4, containing 50% glycerol. The glycerol was removed by a series of dilution/concentration steps prior to the fluorescence measurements. Protein concentrations were determined spectrophotometrically using $\epsilon_{278} = 6.22 \times 10^7$ M^{-1} cm^{-1}.

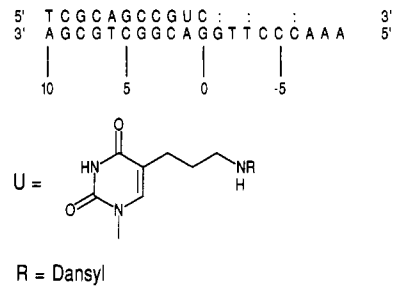

FIGURE 1: Fluorescent 11*/20-mer duplex. U denotes a derivatizable base modified with dansyl chloride. The primer oligonucleotide can be sequentially elongated with Klenow fragment and appropriate dNTP's. The colon denotes the length of the primer in the absence of the next required dNTP. A numbering scheme specifying the position of the derivatizable base is shown.

The DNA oligomer used in most of the studies described here is shown in Figure 1. The synthesis, derivatization, and purification of the dansyl-labeled primer 11-mer (referred to as 11*) and unlabeled template 20-mer oligonucleotides have been described previously (Allen et al., 1989). A second oligonucleotide 20-mer, sequence shown in Figure 2, was also used as a template in some experiments described later. The fluorescent 11*/20-mer duplex shown in Figure 1 was prepared by mixing the 11*-mer (10 μM) with a small molar excess of the 20-mer in a buffer of 50 mM Tris-HCl, pH 7.4. The complex of 11*/20-mer DNA and the Klenow fragment, referred to as 11*/20/KF, was prepared by mixing the 11*/20-mer (10 μM) with Klenow fragment (12 μM) in a buffer of 50 mM Tris-HCl, pH 7.4, containing 1 mM EDTA.

Titration of Labeled 11/20-mer with Klenow Fragment.* Various amounts of the Klenow fragment were added to a solution of 11*/20-mer (10 μM), and the steady-state fluorescence emission intensity was measured at 535 nm with excitation at 320 nm. Klenow fragment was added until there was no further change in the emission intensity. The increase in fluorescence emission intensity versus the amount of added protein was analyzed with a model of free and bound 11*/20-mer in equilibrium, each characterized by a different intrinsic emission intensity. The dissociation constant for the 11*/20/KF complex was varied in order to achieve a best fit to the data using a nonlinear least-squares algorithm.

Primer Strand Elongation. Primer strand elongation was carried out by addition of deoxynucleoside triphosphates (1 mM) to a solution of 11*/20-mer (10 μM), Klenow fragment (12 μM), $MgCl_2$ (3 mM), and Tris-HCl (50 mM, pH 7.4). The dNTP's were chosen according to the template sequence shown in Figure 1. The primer was elongated in a stepwise fashion to 12, 14, or 17 bases in length by the sequential addition of dCTP, dATP, and dGTP, respectively. The resulting DNA–protein complexes are designated 12*/20/KF, 14*/20/KF, and 17*/20/KF. The primer strand was not elongated beyond 17 bases in length in order to retain a 5′ overhang on the template strand. Time-resolved and steady-state fluorescence measurements were made after the addition of each dNTP. A fresh sample was prepared for each fluorescence measurement.

Incorporation of Epoxy-ATP. Epoxy-ATP was generously supplied by Dr. M. Cowart. The labeled 11*-mer (10 μM) was annealed with a small molar excess of the template 20′-mer shown in Figure 2. Note that this template has a different sequence from that shown in Figure 1 and is ac-

```
5' TCGCAGCCGUCGCCCGA(e)    3'
3' AGCGTCGGCAGCGGGCTAAA    5'
```

FIGURE 2: Fluorescent 17*(e)/20′-mer duplex containing epoxy-AMP, denoted A(e), at the 3′ terminus of the primer oligonucleotide and the dansylated uridine base located seven bases upstream from the primer 3′ terminus.

cordingly referred to as 20′-mer. Klenow fragment (12 μM) was added to the 11*/20′-mer solution, followed by $MgCl_2$ (3 mM), dGTP (1 mM), dCTP (1 mM), and epoxy-ATP (1 mM). The primer oligonucleotide was thereby extended to the labeled 17*(e)-mer shown in Figure 2 with a single epoxy-AMP residue at the 3′ terminus and with the dansyl probe seven bases upstream. The resulting DNA–protein complex is referred to as 17*(e)/20′/KF. In some experiments, dATP was used in place of epoxy-ATP as a control. The resulting complex, referred to as 17*/20′/KF, has the dansyl probe at the same position but has a normal AMP residue at the primer terminus.

Time-Resolved Fluorescence Spectroscopy. Samples were excited with the frequency-doubled output of a synchronously mode-locked and cavity-dumped CW dye laser (Coherent 702-CD). The excitation wavelength was in the range 310–328 nm. The pulse duration was <5 ps, and the pulse repetition frequency was 1.87 MHz. The fluorescence was collected at 90° to the excitation beam, passed through a polarizer that could be oriented parallel, perpendicular, or at 54.7° to the vertical excitation polarization, passed through a depolarizer, and finally focused on the slits of a 0.1-m single-grating monochromator (JY H-10). Measurements were made at a number of emission wavelengths. A microchannel plate photomultiplier (Hamamatsu R2809U-01) placed at the exit slit of the monochromator was used to detect the fluorescence, and its output was processed with a time-correlated single photon counting system. The instrument response function was measured by scattering the laser pulses into the detector with a dilute solution of nondairy coffee creamer. The FWHM of the response was 45 ps. Data acquisition and the emission polarizer direction were under computer control. At least 10 000 single photon counts were accumulated in the peak channel of the fluorescence decay curve.

The isotropic fluorescence decay curve was measured with the emission polarizer oriented at 54.7° to the vertical excitation polarization. For anisotropy decay measurements, the emission polarizer was switched between vertical and horizontal directions every 15 s and the two decay curves were accumulated in separate memory segments of a multichannel analyzer. The polarization bias of the detection system was checked with a reference sample whose fluorescence was depolarized. The fluorescence intensity measured with the polarizer in the horizontal direction was multiplied by 1.023 (G factor) to correct for the small polarization bias.

Steady-State Fluorescence Spectroscopy. Steady-state fluorescence excitation and emission spectra were recorded on a Perkin-Elmer Model LS4 or Shimadzu Model 2500 RFU spectrofluorometer. The band-pass was 4 nm for both the excitation and emission monochromators. The steady-state emission spectrum of each sample was recorded before and after the time-resolved fluorescence measurement to check that the sample had not degraded during the measurement.

Data Analysis. (*i*) *Homogeneous Probe Population.* In most cases encountered in this work, the population of dansyl probes could be treated as homogeneous. The fluorescence decay of the dansyl probe can be complex, even for a homogeneous population, due to emission from multiple excited states or solvent relaxation. The isotropic fluorescence decay was accordingly analyzed with a multiexponential model:

$$I(t) = g(t) \otimes K(t) \tag{1}$$

and

$$K(t) = \sum_{j=1}^{N} \alpha_j \exp(-t/\tau_j) \tag{2}$$

where $g(t)$ is the instrument response function, ⊗ denotes convolution of two functions, α_j is the fractional amplitude associated with each fluorescence lifetime τ_j, and N is the number of decay components. Further, $\sum_{j=1}^{N} \alpha_j = 1$. The convolution integral was calculated numerically by using Simpson's rule. The parameters α_j and τ_j were optimized for a best fit of eq 1 and 2 to the data by using a nonlinear least-squares method (Bevington, 1969). The goodness of fit was judged by the reduced χ^2 value (χ_r^2) and by examination of the weighted residuals. The uncertainty of the best-fit parameters was calculated from the diagonal elements of the error matrix, thereby taking into account both the precision of the experimental data and the correlation between the adjustable parameters (Bevington, 1969). The average fluorescence lifetime was defined as

$$\bar{\tau} = \sum_{j=1}^{N} \alpha_j \tau_j \tag{3}$$

The fluorescence anisotropy decay data was analyzed according to

$$I_{\parallel}(t) = g(t) \otimes \{[1 + 2r(t)]K(t)\} \tag{4}$$

and

$$I_{\perp}(t) = g(t) \otimes \{[1 - r(t)]K(t)\} \tag{5}$$

where

$$r(t) = \sum_{k=1}^{M} \beta_k \exp(-t/\phi_k) \tag{6}$$

$I_{\parallel}(t)$ and $I_{\perp}(t)$ are the time-resolved intensities of the parallel and perpendicular polarization components of the fluorescence, respectively, and $r(t)$ is the time-dependent fluorescence anisotropy. The anisotropy is represented in eq 6 by a multiexponential model to account for various types of motion, such as internal rotation of the probe and overall tumbling. There are M anisotropy decay components, β_k is the limiting anisotropy of component k, and ϕ_k is the corresponding decay time. The total limiting anisotropy is r_0, where $r_0 = \sum_{k=1}^{M} \beta_k$. The parameters describing $K(t)$ were determined as described above and were kept fixed, whereas the parameters β_k and ϕ_k were optimized for a simultaneous best fit of eq 4–6 to $I_{\parallel}(t)$ and $I_{\perp}(t)$ (Cross & Fleming, 1984). Since the population of dansyl probes is homogeneous, each lifetime component in eq 2 is associated with every anisotropy decay component in eq 6. The goodness of fit was judged as described above.

The angular range of the restricted internal rotation of the dansyl probe was calculated by using a model of isotropic diffusion within a cone (Kinosita et al., 1977). The semiangle of the cone was given by

$$\theta = \cos^{-1}\{(1/2)[(1 + 8S)^{1/2} - 1]\} \tag{7}$$

where $S = (\beta_2/r_0)^{1/2}$ is the generalized order parameter (Lipari & Szabo, 1980).

(*ii*) *Heterogeneous Probe Population.* In some cases encountered in this study, heterogeneity of the dansyl probe population causes observable effects in the fluorescence anisotropy decay. When the dansyl probe is located at certain positions within the primer oligonucleotide, the multiple binding modes of the DNA–protein complex give rise to a

Table I: Fluorescence Lifetime Analysis[a]

sample	probe position	τ_1 (ps) (±50)	τ_2 (ns) (±0.3)	τ_3 (ns) (±0.3)	α_1 (±0.015)	α_2 (±0.015)	α_3 (±0.015)	χ_r^2	$\bar{\tau}$ (ns) (±0.30)
11*	+1	154	3.6	8.5	0.220	0.488	0.292	1.07	4.30
11*/20	+1	280	3.2	9.8	0.172	0.495	0.333	1.05	4.88
11*/20/KF	+1	355	4.0	13.4	0.179	0.350	0.471	0.99	7.75
12*/20/KF	+2	378	3.8	10.8	0.169	0.572	0.259	1.08	5.01
14*/20/KF	+4	428	4.0	10.7	0.169	0.554	0.277	1.04	5.25
17*/20/KF	+7	311	3.4	11.4	0.218	0.610	0.172	1.14	4.13
17*/20′/KF	+7	489	3.8	13.0	0.199	0.678	0.123	1.11	4.28
17*(e)/20′/KF	+7	289	3.7	11.1	0.256	0.622	0.122	1.17	3.70

[a] λ_{ex} = 317 nm, λ_{em} = 535 nm, 20 °C, emission polarizer at 54.7°. Number in parentheses are 95% confidence intervals.

mixture of solvent-exposed and protein-associated dansyl probes. The anisotropy decay is then represented by (Ludescher et al., 1987)

$$r(t) = f_e(t)r_e(t) + f_b(t)r_b(t) \quad (8)$$

where $f_e(t)$ is the fraction of fluorescence at time t due to the exposed dansyl probes, $r_e(t)$ describes the anisotropy decay of the exposed probes, and $f_b(t)$ and $r_b(t)$ are the corresponding quantities for the buried dansyl probes. This equation assumes that the exposed and buried probes are not interconverting on the fluorescence time scale, which is reasonable in the present case since the interconversion between the different modes of the DNA–protein complex is estimated to occur in the millisecond time range (Freemont et al., 1989).

The function $f_e(t)$ is given by

$$f_e(t) = x_e\sum_{j=1}^{N}\alpha_{je}\exp(-t/\tau_{je})/[x_e\sum_{j=1}^{N}\alpha_{je}\exp(-t/\tau_{je}) + x_b\sum_{j=1}^{N}\alpha_{jb}\exp(-t/\tau_{jb})] \quad (9)$$

where x_e and x_b are the mole fractions of exposed and buried probes, respectively, and the e and b subscripts on the α_j and τ_j parameters refer to exposed and buried probes, respectively. The number of decay components, N, is the same as for the homogeneous population of eq 2. The α_{je}, α_{jb}, τ_{je}, and τ_{jb} parameter are also defined as in eq 2. The exposed and buried probes are assumed to have the same extinction coefficients and radiative rate constants. A similar expression applies for $f_b(t)$. Note that $x_e + x_b = 1$. The anisotropy decay functions $r_e(t)$ and $r_b(t)$ are each given by expressions of the form shown in eq 6. The parameters appearing in eq 6 are given an additional subscript to denote each probe population.

Results

Steady-State Fluorescence Spectra. The steady-state fluorescence excitation and emission spectra of the labeled 11*-mer single strand are shown in Figure 3. The emission maximum is at 535 nm, and the excitation maximum is at 340 nm. The spectra of the 11*/20-mer are similar to those shown in Figure 3. The steady-state emission spectra of the series of DNA–protein complexes have been reported previously (Allen et al., 1989).

Fluorescence Titration of the 11/20-mer Duplex with Klenow Fragment.* The titration curve is shown in Figure 4. The dansyl emission intensity at 535 nm increases as the Klenow fragment is added to the 11*/20-mer duplex and reaches an apparent limit when 1.0 equiv of protein has been added, showing that a 1:1 complex is formed. Nonlinear least-squares fitting of the titration curve yields a K_D value of 7.9 nM for the 11*/20/KF complex in 50 mM Tris-HCl, pH 7.4, containing 1 mM EDTA at 20 °C.

The 11*/20/KF complex examined by time-resolved fluorescence spectroscopy contained 1.2 equiv of Klenow fragment. The titration data presented in Figure 4 demonstrate that all the DNA is bound to the Klenow fragment under these conditions.

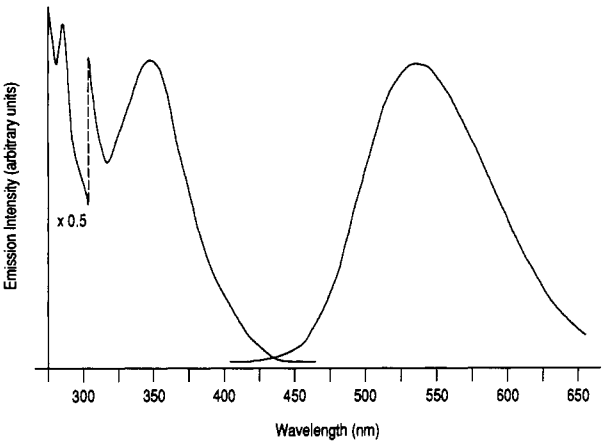

FIGURE 3: Steady-state fluorescence excitation (at left) and emission (at right) spectra of the 11*-mer oligonucleotide (10 μM) in 50 mM Tris-HCl, pH 7.4, at 20 °C. The band-pass is 4 nm in both spectra.

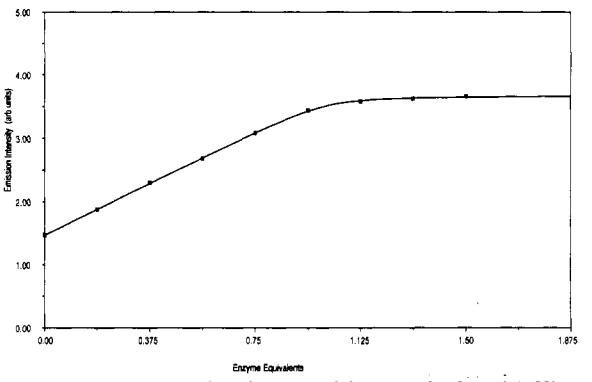

FIGURE 4: Fluorescence titration of 11*/20-mer DNA with Klenow fragment. The emission intensity at 535 nm is plotted against the molar equivalent of Klenow fragment added to the 11*/20-mer (10 μM) in 50 mM Tris-HCl, pH 7.4 at 20 °C. The points are experimental data, and the smooth line is the best fit to a model of free and bound 11*/20-mer in a two-state equilibrium with K_D = 7.9 nM.

Fluorescence Lifetimes. Three decay components (N = 3) are required to obtain a good fit of eq 1 and 2 to the isotropic fluorescence decay of the 11*-mer single strand and 11*/20-mer duplex in aqueous solution. The best-fit parameter values are constant, within experimental error, on all the time scales used in the measurements (from 7 to 90 ps/channel). The best-fit parameters are presented in Table I. Good fits are obtained in all cases, as shown by the χ_r^2 values presented in Table I.

The results obtained for the 11*-mer single strand and 11*/20-mer duplex are very similar (Table I). The dependence of the isotropic decay parameters of the 11*/20-mer duplex on the emission wavelength is presented in Table II. The three

Table II: Fluorescence Lifetimes of the 11*/20-mer versus Emission Wavelength[a]

λ_{em} (nm)	τ_1 (ps) (±50)	τ_2 (ns) (±0.3)	τ_3 (ns) (±0.3)	α_1 (±0.015)	α_2 (±0.015)	α_3 (±0.015)	χ_r^2	$\bar{\tau}$ (ns) (±0.30)
515	303	3.4	10.4	0.241	0.453	0.306	1.10	4.78
535	280	3.2	9.8	0.172	0.495	0.333	1.05	4.88
560	288	3.1	9.2	0.122	0.510	0.368	1.06	5.01

[a] λ_{ex} = 317 nm, 20 °C, emission polarizer at 54.7°. Numbers in parentheses are 95% confidence intervals.

Table III: Anisotropy Decay Parameters[a]

sample	probe position	ϕ_1 (ps) (±50)	ϕ_2 (ns)	β_1 (±0.010)	β_2 (±0.010)	r_0 (±0.020)	χ_r^2	θ (deg) (±3)
11*	+1	242	2.3 ± 0.4	0.137	0.125	0.257	1.04	39
11*/20	+1	591	9.1 ± 0.5	0.144	0.120	0.264	1.06	40
11*/20/KF	+1	910	56 ± 3	0.044	0.232	0.276	1.04	19
12*/20/KF	+2	389	54 ± 3	0.084	0.202	0.286	1.12	27
14*/20/KF	+4	493	57 ± 3	0.094	0.169	0.263	1.10	31
17*/20/KF	+7	685	>500[b]	0.152	0.104	0.256	1.04	43
17*/20′/KF	+7	799	>500[b]	0.162	0.107	0.269	1.13	43
17*(e)/20′/KF	+7	786	87 ± 10	0.152	0.142	0.294	1.15	39

[a] λ_{ex} = 317 nm, λ_{em} = 535 nm, 20 °C. Numbers in parentheses or preceded by ± are 95% confidence intervals. [b] "Dip and rise" in the anisotropy curve.

lifetimes do not depend on the emission wavelength, but the amplitudes vary slightly with wavelength. The isotropic decay parameters were also determined at three different excitation wavelengths (310, 317, and 328 nm), and the same values were found in each case (data not shown).

Three decay components are also required to fit the isotropic fluorescence decay of the DNA–protein complexes (Table I). In the case of the 11*/20/KF complex, the lifetime, τ_1, and amplitude, α_1, do not differ significantly from the values found for the free DNA molecules. However, the other two lifetimes increase upon complex formation, particularly the longest lifetime, τ_3. Further, the amplitude α_3 increases upon complex formation, while α_2 decreases. The average fluorescence lifetime, defined in eq 3, consequently increases substantially upon binding of the 11*/20-mer to Klenow fragment. The steady-state emission intensity also increases substantially upon binding (data not shown).

The fluorescence lifetimes of the dansyl probe in each of the DNA–protein complexes obtained by elongation of the primer strand are presented in Table I. The lifetime, τ_1, and amplitude, α_1, remain approximately constant in each of the complexes. However, the other decay parameters change as the probe is positioned further upstream from the 3′ terminus of the primer strand by stepwise primer elongation (Table I). In particular, note that the average fluorescence lifetime decreases as the probe moves further upstream from the primer 3′ terminus.

The dependence of the decay amplitudes on the excitation and emission wavelengths in each of the DNA–protein complexes is essentially the same as that described above for the free 11*/20-mer duplex.

Fluorescence Anisotropy Decay. The fluorescence anisotropy decay of the 11*/20-mer duplex in aqueous solution is shown in Figure 5. The data for the 11*-mer single strand and 11*/20-mer duplex were analyzed with eqs 4–6, which assume a homogeneous population of dansyl probes. This assumption should be valid for the unbound 11*-mer and 11*/20-mer in aqueous solution. Two decay components are required to fit the anisotropy decay of these molecules. The resulting anisotropy decay parameters are constant, within experimental error, on all the time scales used in the measurements (7–90 ps/channel). The best-fit parameter values are presented in Table III. Good fits to the experimental data are obtained in all cases, as indicated by the χ_r^2 values shown in Table III. The amplitude of internal rotation of the dansyl probe calculated from eq 7 is also included in Table III.

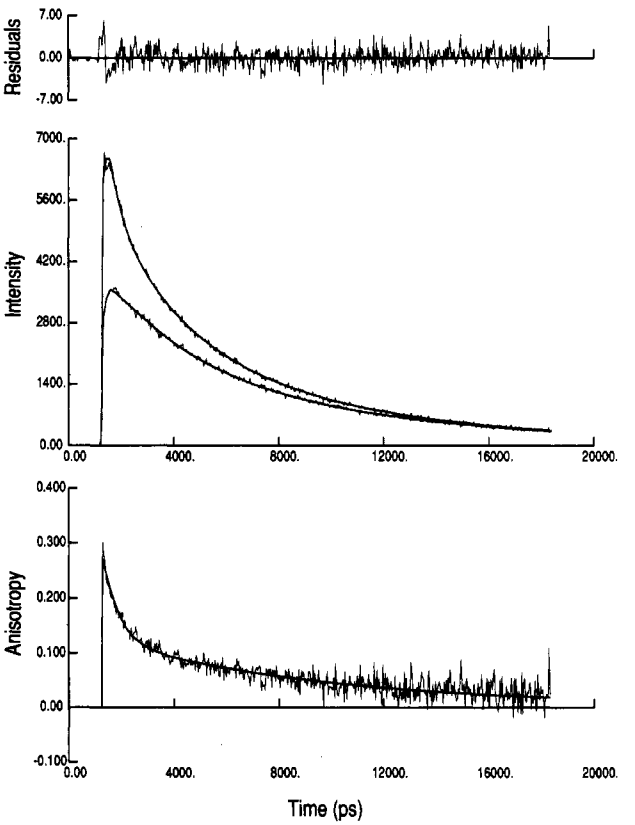

FIGURE 5: Fluorescence anisotropy decay of 11*/20-mer (10 μM) in 50 mM Tris-HCl, pH 7.4 at 20 °C. $I_{\parallel}(t)$ and $I_{\perp}(t)$ are shown in the center panel, $r(t)$ is in the lower panel, and the weighted residuals for the difference curve $I_{\parallel}(t) - I_{\perp}(t)$ are shown in the upper panel. The smooth lines are best-fit curves obtained by using eqs 4–6, as described in the text.

The anisotropy decay of the DNA–protein complexes was also analyzed with eq 4–6. This analysis may not be exact in these cases, since heterogeneous probe populations can occur with the DNA–protein complexes due to multiple modes of binding, especially if the fluorescence decay and motional characteristics of the probe are different in each mode. However, if the probe environment is similar in each binding mode of the complex and if one mode of binding predominates, then the probe population will be essentially homogeneous, and eq 4–6 will be appropriate. This turns out to be the case with

most of the DNA–protein complexes studied. So, for example, in the case of the 11*/20/KF, 12*/20/KF, and 14*/20/KF complexes, the anisotropy decay can be adequately represented by eq 4–6 with two decay components. The resulting best-fit parameters are presented in Table III. These parameters are weighted in favor of the most abundant form of the DNA–protein complex, which is later shown to be the form in which the DNA primer 3′ terminus is bound at the polymerase active site. Note that the longer anisotropy decay time, ϕ_2, has approximately the same value in each complex.

The anisotropy decay parameters were determined at various excitation (310, 317, and 328 nm) and emission (515, 535, and 560 nm) wavelengths. The same results were found in each case, implying that the anisotropy decay behavior is independent of the excitation or emission wavelength. The data in Table III are for one particaular combination, excitation at 317 nm and emission at 535 nm.

The approximate analysis based on a homogeneous probe population fails in the case of the 17*/20/KF complex. The anisotropy decay of this complex is more complicated than can be represented with a homogeneous probe population. The anisotropy decreases with time during the first 10 ns of the decay, then increases during the next 20 ns, and thereafter decreases with time (Figure 6A). When the data are analyzed assuming homogeneity of the probe population, the best-fit value of ϕ_2 is anomalously large (Table III). This occurs because the model expression in eq 6 cannot represent the anisotropy curve when every fluorescence lifetime is associated with each anisotropy decay time and when the β values are all positive. The best fit that can be achieved with these constraints is to make the calculated curve very flat at long times, by making ϕ_2 very large. The value of ϕ_2 obtained under these conditions is very sensitive to the G factor used to correct $I_\perp(t)$. However, the recovered value of ϕ_2 is not physically significant in this case, since the apparently large value is actually an artifact of the homogeneous probe approximation. An anisotropy decay curve that exhibits a high initial value and that rises at later times, such as observed with the 17*/20/KF complex, is indicative of a heterogeneous probe population (Ludescher et al., 1987). The anistotropy curve of the 17*/20/KF complex can be reproduced by using a reasonable value for ϕ_2 when the heterogeneity of the probe population is taken into account, as shown below. The magnitude of ϕ_2 obtained by assuming homogeneity, as reported in Table III, actually reports on the existence of heterogeneity in the probe population in the 17*/20/KF complex. The 11*/20/KF, 12*/20/KF, and 14*/20/KF complexes do not exhibit a large degree of heterogeneity in the probe population, and the assumption of a homogeneous probe population accordingly works well since the same value of ϕ_2 is obtained in each sample.

The anisotropy decay of the 17*/20/KF complex was analyzed according to eq 8 in order to account for the heterogeneity of the probe population. This equation involves a large number of parameters, not all of which can be simultaneously determined by fitting the anisotropy decay of the 17*/20/KF complex. However, the calculated anisotropy curve was found to be most sensitive to the values of α_{3e}, τ_{3e}, α_{3b}, τ_{3b}, β_{1e}, and β_{1b}, and was less sensitive to the value of the remaining parameters. This group of parameters was varied in order to fit the anisotropy decay of the 17*/20/KF complex. The remaining parameters could be independently estimated. For example, the exposed probe population in the 17*/20/KF complex should behave similarly to the probe in the unbound 11*/20-mer duplex, which represents a single solvent-exposed

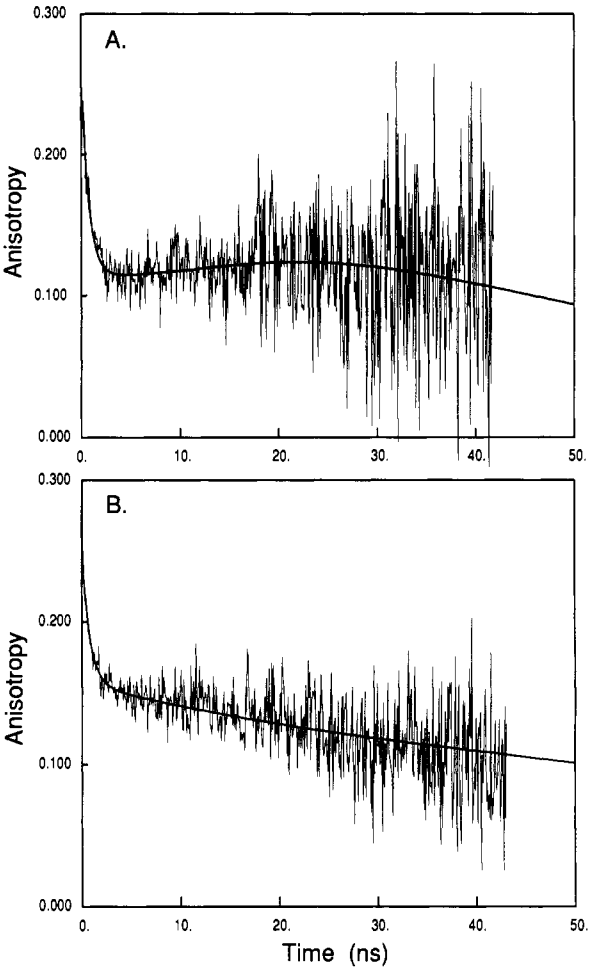

FIGURE 6: (A) Fluorescence anisotropy decay of the 17*/20/KF complex in 50 mM Tris-HCl, pH 7.4 at 20 °C. The smooth solid line is the best fit (χ_r^2 = 1.08) of eq 8, which assumes a mixture of exposed and buried dansyl probes. The parameter values used in the calculation are as follows: τ_{1e} = 350 ps, τ_{2e} = 3.4 ns, τ_{3e} = 7.5 ns, α_{1e} = 0.22, α_{2e} = 0.61, α_{3e} = 0.17, ϕ_{1e} = 749 ps, ϕ_{2e} = 57 ns, β_{1e} = 0.169, β_{2e} = 0.096, τ_{1b} = 350 ps, τ_{2b} = 5.5 ns, τ_{3b} = 15.6 ns, α_{1b} = 0.16, α_{2b} = 0.45, α_{3b} = 0.39, ϕ_{1b} = 1.0 ns, ϕ_{2b} = 57 ns, β_{1b} = 0.040, β_{2b} = 0.234, and x_b = 0.120. The parameters α_{3e}, τ_{3e}, α_{3b}, τ_{3b}, β_{1e}, β_{2e}, and x_b were adjusted for a best fit to the data, and the other parameters were kept fixed. See text for details. (B) Fluorescence anisotropy decay of the complex of 17*/20-mer with the D355A, E357A mutant Klenow fragment. The smooth solid line is the best fit (χ_r^2 = 1.10) with the same parameters as in (A) except for x_b = 0.031. See text for details.

probe population. Hence, N, M, α_{2e}, τ_{je} (j = 1, 2), r_0, and ϕ_{1e} were set to the corresponding values determined above for the unbound 11*/20-mer (Tables I and III). However, ϕ_{2e} was set to 57 ns, the value obtained for the other DNA–protein complexes. In the case of the buried probes in 17*/20/KF, the corresponding parameters were set to the values found for the 11*/20/KF complex (Tables I and III), in which the dansyl probe can be treated as a homogeneous buried population. Equation 8 was fitted to the anisotropy decay of 17*/20/KF by adjusting x_b and the variable parameters noted above, using a nonlinear least-squares method (Bevington, 1969). A typical best-fit curve is shown in Figure 6A. The fit is good, as indicated by the χ_r^2 value. The best-fit value of x_b is 0.120, and the confidence range is ±0.015, which is mainly determined by the degree of correlation between the adjustable parameters.

Effect of Epoxy-Terminated Primer Strand. The fluorescence lifetimes and anisotropy decay parameters for the 17*(e)/20′/KF complex are presented in Tables I and III,

respectively. The analysis again assumes a homogeneous probe population. The lifetimes and their associated amplitudes are essentially identical with those of the unmodified 17*/20-mer duplex bound to the Klenow fragment (Table I). However, in the 17*(e)/20′/KF complex, the anisotropy decay does not exhibit a pronounced "dip and rise". The value of ϕ_2 recovered from the analysis is similar to the value obtained for the 11*/20/KF, 12*/20/KF, and 14*/20/KF complexes (Table III). The degree of probe heterogeneity is apparently reduced in this complex compared with the corresponding complex formed with unmodified 17*/20-mer. In a control experiment, dATP was used in place of epoxy-ATP to extend the 11*-mer primer, thereby placing a normal dAMP residue at the 3′ terminus of the primer strand, with the dansyl probe seven bases upstream as before. The anisotropy decay of this 17*/20′/KF complex does exhibit the "dip and rise". Further, the apparent value of ϕ_2 obtained with the assumption of a homogeneous probe population is again anomalously large (Table III). The anisotropy decay behavior of the 17*/20/KF and 17*/20′/KF complexes is essentially identical, showing that the different primer and template sequences in the two complexes have no effect on the decay. The different anisotropy decay observed for the 17*(e)/20′/KF complex, noted above, is therefore due to the epoxy-AMP residue at the 3′ terminus of the primer strand and not to the different sequence of the primer and template strands.

The anisotropy decay curve of the 17*(e)/20′/KF complex was also analyzed according to eq 8. All the parameters, with the exception of x_b, were set equal to the values obtained from the analysis of the 17*/20/KF complex discussed earlier. The mole fraction x_b was then varied in order to fit the anisotropy decay of the 17*(e)/20′/KF complex: x_b was found to be 0.040 ± 0.015, 3 times lower than for the unmodified 17*/20-mer bound to the Klenow fragment. The small residual amount of buried probes explains why the apparent value of ϕ_2 obtained by assuming a homogeneous probe population is somewhat larger than the value obtained for the 11*/20/KF, 12*/20/KF, and 14*/20/KF complexes (Table III).

Effect of Site-Directed Mutagenesis of the Klenow Fragment. The mutant Klenow fragment D355A, E357A was used to prepare the 17*/20/KF complex. This mutant protein has normal polymerase activity but lacks 3′→5′ exonuclease activity (Derbyshire et al., 1988). The anisotropy decay of this complex is shown in Figure 6B. The "dip and rise" is not observed in this case, and the value of ϕ_2 recovered from eq 4–6 is 69 ± 3 ns, which is very similar to the value obtained for the 11*/20/KF, 12*/20/KF, and 14*/20/KF complexes prepared with the wild-type protein. The degree of probe heterogeneity in this DNA–protein complex is therefore reduced compared to the corresponding complex prepared with the wild-type protein. This was confirmed by fitting the anisotropy decay according to eq 8, keeping all the parameters except x_b equal to the values previously determined for the 17*/20/KF complex prepared with the wild-type protein. The best-fit value of x_b is found to be 0.031 ± 0.015. The number of buried dansyl probes in the 17*/20/KF complex prepared with the mutant protein is therefore significantly reduced compared to the corresponding complex obtained with the wild-type protein.

Discussion

A Fluorescence Approach to DNA–Polymerase Interactions. A fluorescent DNA duplex was synthesized for the present study by incorporating a derivatizable uridine base in the primer oligonuleotide. The propylamine substituent at the 5-position of the uridine base was then reacted with dansyl chloride to yield the labeled 11*-mer shown in Figure 1. Substitution at the 5-position allows the uridine base to base pair with the opposing adenine base on the template strand and allows the linker arm and probe to project into the major groove of the B-DNA double helix. The linker and the probe therefore do not prevent hybridization of the primer and template strands and cause only minimal structural distortion of the resulting DNA duplex. Furthermore, *E. coli* DNA polymerase I utilizes uridine nucleotides substituted at the 5-position as substrates (Dale et al., 1973).

The fluorescent 11*/20-mer duplex binds tightly to the Klenow fragment, with K_D = 7.9 nM, and forms a 1:1 complex (Figure 4). The dissociation constant is very similar to that reported for the same 11/20-mer duplex without the linker and probe, K_D = 5 nM (Kuchta et al., 1987). The propyl linker and dansyl group therefore do not seriously perturb the interaction of the DNA duplex with the Klenow fragment. The 11*/20-mer is also an active substrate for both the polymerization and 3′→5′ exonuclease activities of the Klenow fragment (Allen et al., 1989). This fluorescent duplex thus appears to be a suitable model for studying the interaction of DNA with the Klenow fragment.

An attractive feature of the fluorescent duplex for the present study is that the position of the dansyl probe within the duplex can be readily varied. The template strand in the 11*/20-mer duplex is designed such that the primer strand can be elongated in discrete steps by the polymerization activity of the Klenow fragment upon the addition of the appropriate dNTP's to the solution, thereby positioning the dansyl probe at various known distances upstream from the primer 3′ terminus (Figure 1). The primer is sequentially extended to 12, 14, and 17 bases in length, thereby locating the probe at positions +2, +4, and +7 relative to the 3′ terminus of the primer strand. The numbering scheme is shown in Figure 1, where the probe distance from the primer 3′ terminus is measured in bases, with positive values indicating the duplex portion of the substrate. Note that the origin is always defined to be at the 3′ terminus of the primer strand and that the template strand has a 5′ overhang in each of the DNA–protein complexes.

The fluorescence decay of the dansyl probe can be studied at various positions within the DNA–protein complex by this approach. The probe in effect "walks through" the complex in a number of discrete steps, and its local environment at each point is reflected in its fluorescence decay behavior. If the structure of the complex is assumed to be the same in each case, then a map of the DNA–protein contacts within the complex is obtained, which is useful in footprinting the complex. This assumption should be valid for the Klenow fragment since its interaction with DNA is not strongly sequence-dependent. However, there are two potential limitations. First, the binding affinity may be reduced as the template overhang is shortened by elongation of the primer strand. The presence of free DNA in the solution would then complicate the interpretation of the fluorescence decay data. However, the dissociation constant increases by only a modest amount as a 9/20-mer DNA oligomer (K_D = 5 nM) is extended to a 17/20-mer (K_D = 25 nM) by the Klenow fragment (Kuchta et al., 1987). A similar change should apply to the elongation of the 11*/20-mer (K_D = 7.9 nM) to the 17*/20-mer, but such an increase in K_D would not produce a significant concentration of free DNA under the conditions of the present experiments. Second, a blunt-ended duplex can bind to the Klenow fragment in two orientations, which could place the dansyl probe in different environments. An overhang at the 5′ end of the

template strand is present in each of the DNA substrates to avoid this possibility.

It is important to ensure that the DNA substrate is not degraded by the 3′→5′ exonuclease activity of the Klenow fragment during the 30-min accumulation of the fluorescence decay data. EDTA is therefore added to the 11*/20/KF solution to remove divalent metal ions from the enzyme, required for the 3′→5′ exonuclease activity. This approach cannot be used with the complexes obtained by primer elongation, since divalent metals are also required for the polymerase activity of the enzyme. In the primer elongation reactions, a 100-fold molar excess of the appropriate dNTP's is added, such that any 3′-terminal nucleotide excised from the primer strand by the exonuclease activity is rapidly reinserted by the polymerase activity from the large pool of dNTP's available in solution. In this idling/turnover mode of the enzyme, the primer strand maintains a constant length, and the probe position is accordingly unchanged, until the dNTP pool is exhausted (Brutlag & Kornberg, 1972; Mizrahi et al., 1986). Since the emission maximum of the dansyl probe has a characteristic position at each primer strand length (Allen et al., 1989), the steady-state fluorescence spectrum of each freshly prepared sample was recorded before and after the acquisition of the time-resolved fluorescence data to check whether the primer strand had degraded during the measurement. The samples were found to be stable for several hours.

Photophysics of the Dansyl Probe. Three distinct lifetimes are observed in the fluorescence decay of the dansyl probe attached to the oligonucleotide (Tables I and II). Two lifetimes have been previously reported for the fluorescence decay of dansyl-modified proteins (Lambooy et al., 1982; Chen & Scott, 1985), and these correspond closely to the two longer lifetimes found here, τ_2 and τ_3. The excitation and emission spectra measured in the present study (Figure 3) are also similar to those reported for dansyl-modified ovalbumin (Chen & Scott, 1985). The shortest lifetime, τ_1, has not been previously reported. Since this lifetime is in the subnanosecond range and has the smallest amplitude in the fluorescence decay, it has probably escaped detection in earlier studies due to lower time resolution. This lifetime component is blue-shifted with respect to the two longer lifetime components (Table II). The possibility that τ_1 represents an emission from the nucleic acid bases can be ruled out since the amplitude α_1 is found to be the same for the 11*-mer single strand and 11*/20-mer duplex (Table I), even though the duplex contains more bases. Furthermore, the bases have very little absorption in the 310–328-nm wavelength range used to excite the samples. It is unlikely that τ_1 is due to an impurity since the purified 11*-mer oligonucleotide elutes as a single peak by HPLC and the buffer is free of fluorescent impurities. It appears that all three lifetimes are due to the dansyl probe.

Since the fluorescence quantum yield increases when the dansyl group is located in a hydrophobic environment (Chen, 1967), the fluorescence lifetimes should also increase. The lifetimes are found to be the same for the 11*-mer single strand and 11*/20-mer duplex in aqueous solution (Table I), suggesting that the dansyl probe is located in an environment of similar polarity in both molecules. The degree of exposure of the probe to the aqueous solvent may therefore be the same in the single-stranded and duplex molecules. However, the lifetimes τ_2 and τ_3 do increase when the 11*/20-mer binds to the Klenow fragment (Table I), suggesting that the probe is in a more hydrophobic environment in the DNA–protein complex. Also, the dansyl emission intensity increases, and the emission maximum shifts to shorter wavelengths upon formation of this complex (Allen et al., 1989). The lifetime τ_1 is apparently insensitive to the probe environment since it does not change upon binding or elongation of the primer strand (Table I).

Qualitative information on the polarity within various regions of the DNA–protein complex can be inferred from the variation in the fluorescence lifetimes that occur as the probe is positioned further upstream of the primer 3′ terminus by stepwise elongation of the primer strand. The average lifetime is longest at position +1 in the complex, implying that the region around the 3′ terminus of the DNA primer strand is the most hydrophobic. This suggests that the aqueous solvent is excluded from the polymerase active site, at least when the DNA substrate is bound to the protein. The average lifetime is shorter at positions +2 and +4, but is still longer than in the unbound 11*-mer or 11*/20-mer. This region of the DNA–protein complex is less hydrophobic than the region around the primer terminus, but is still more hydrophobic than the probe environment in aqueous solution. When the probe is located seven bases upstream from the primer terminus, the average lifetime is similar to, but somewhat shorter than, that observed in the unbound 11*-mer or 11*/20-mer. The probe is apparently exposed to the solvent at this position in the complex, and its fluorescence is also quenched, perhaps due to its proximity to the protein. The polarity changes detected with the lifetime measurements reported here are consistent with the changes detected in the steady-state fluorescence spectrum of the dansyl probe (Allen et al., 1989).

Rotational Dynamics of the Probe. For a homogeneous fluorophore population, the decay of the fluorescence polarization anisotropy is governed by the reorientation of the fluorophore on the time scale of the fluorescence decay. The anisotropy decay of the unbound 11*-mer and 11*/20-mer molecules can be well represented by two-exponential decay components. The longer decay time, ϕ_2, is in the nanosecond range and is larger for the 11*/20-mer duplex than for the 11*-mer single strand (Table III). Since ϕ_2 increases as the molecular weight of the DNA molecule increases, this anisotropy decay component can be assigned to overall tumbling motions. The other anisotropy decay time, ϕ_1, is too short to represent overall motion of the DNA and is therefore assigned to a restricted internal rotation of the dansyl probe relative to the DNA molecule.

Only a single anisotropy decay time is associated with the overall tumbling of the 11*-mer single strand and 11*/20-mer duplex. The tumbling motion of these molecules therefore appears to be effectively isotropic. The rate of tumbling of the 11*-mer and 11*/20-mer oligonucleotides about different molecular axes is probably different, but these differences are too small to resolve experimentally and the apparent tumbling time ϕ_2 is an average of the individual tumbling times. The tumbling of the 11*/20-mer duplex is slower than that of the 11*-mer single strand, which reflects both the increased diameter of the duplex and the 5′ overhang on the template strand.

In addition to overall motion on the nanosecond time scale, the dansyl probe also reorients on the picosecond time scale due to a restricted internal rotational motion. In the free 11*-mer single strand, this motion has a correlation time of 242 ps and a large angular range (Table III). The angular range is estimated from a cone model of restricted isotropic diffusion (Kinosita et al., 1977), which yields a cone semiangle of 39°. This motion could potentially involve rotation of the rigid dansyl fluorophore about the C–N single bond connecting

it to the linker, as well as rotations about the flexible C–C single bonds in the linker itself. These latter motions would rotate the probe through a large angular range by virtue of a lever arm effect.

The correlation time increases from 242 ps in the 11*-mer single strand to 591 ps in the 11*/20-mer duplex, although the range of motion remains the same (Table III). The major groove of the double helix is apparently large enough to accommodate the large-amplitude internal rotation of the dansyl group and linker. The increase in the correlation time, which is significant since it lies outside the error range associated with each value, indicates that the internal rotation of the dansyl probe is slower in the duplex, perhaps due to interactions between the probe or linker and groups within the major groove of the double helix.

The anisotropy decay of the 11*/20/KF, 12*/20/KF, and 14*/20/KF complexes can also be treated with a homogeneous model with two modes of probe motion. Further, the decay time ϕ_2 has the same value in each of these complexes (Table III), which is consistent with isotropic tumbling of the DNA–protein complex. The tumbling of these complexes is much slower than that of the unbound DNA, which reflects the larger size of the protein. The tumbling time reported by the dansyl probe is independent of its position within the DNA–protein complex. Further, the tumbling time of the complex does not depend on the position of the protein on the DNA.

The short decay time, ϕ_1, is also detected in the anisotropy decay of the DNA–protein complexes, showing that the internal rotation of the dansyl probe persists when the DNA is bound to the protein. However, the angular range of rotation is drastically reduced when the 11*/20-mer binds to the Klenow fragment, since the cone semiangle decreases from 40° to 19° (Table III). This implies that the internal rotation of the dansyl probe is subjected to steric constraints within the DNA–protein complex, presumably due to interaction between the probe and the protein. Further, the correlation time for internal rotation increases from 591 ps in the unbound 11*/20-mer to 910 ps in the 11*/20/KF complex (Table III), showing that the internal rotation is also retarded by the interactions between the probe and the protein. These changes in the internal rotation dynamics of the probe that occur upon binding of the 11*/20-mer to the protein indicate that there is close contact between the protein and the 3′-terminal region of the DNA primer strand.

The internal rotational motion of the dansyl probe, like the fluorescence decay, is sensitive to the position of the probe within the DNA–protein complex (Table III). When the probe is located two bases upstream from the 3′ terminus of the primer strand, the cone semiangle increases to 27°, and the correlation time decreases to 389 ps (Table III). Both changes indicate that there is less interaction between the probe and the protein at this position than at position +1 in the DNA–protein complex. The correlation time is actually shorter than observed in the unbound 11*/20-mer. The difference is not large but is nevertheless significant in view of the error associated with ϕ_1 (Table III). One possible explanation for this difference is that the degree of interaction between the probe and the DNA double helix is reduced in the DNA–protein complex. The probe–DNA interaction does appear to influence the correlation time of internal rotation of the probe in the unbound DNA molecules, as noted earlier. The probe–DNA interactions are still present to some degree in the 12*/20/KF complex, since the correlation time for internal rotation is larger than in the unbound 11*-mer, which exhibits the fastest rotation of the dansyl probe and therefore presumably the least degree of interaction between the probe and the DNA (Table III). When the probe is four bases upstream from the primer 3′ terminus, the range of motion increases further (cone semiangle 31°), indicating a further reduction in the steric constraints to internal rotation of the probe. Also, the correlation time for internal rotation is still shorter than observed in the unbound duplex DNA (Table III). When the probe is seven bases upstream, the correlation time and angular range of internal rotation are essentially the same as found for the unbound 11*/20-mer duplex (Table III). The probe is evidently no longer in contact with the protein at this position within the DNA primer strand. The emission spectrum of the probe at this position is identical with that of the free 11*/20-mer duplex, also implying that the probe is not in contact with the protein (data not shown).

Fluorescence Footprinting. As discussed above, the probe is found to be interacting with the protein at positions +1, +2, and +4 in the complex, but there is no interaction at position +7. This "fluorescence footprinting" technique thus implies that between five and six bases of the primer strand upstream of the 3′ terminus are in contact with the protein, which agrees with the results of the steady-state fluorescence experiments (Allen et al., 1989). These results are consistent with chemical footprinting data, which imply an 8 base pair contact distance (Joyce & Steitz, 1987). The length of the linker arm could account for the difference between the fluorescence and chemical footprints.

The fluorescence footprinting technique used here also provides information on the molecular environment within the DNA–protein complex. The interior of the DNA–protein complex is shown to be hydrophobic, especially around the region of the 3′ terminus of the DNA primer strand. This suggests that binding of DNA in the large cleft in the C-terminal domain of the protein results in exclusion of the aqueous solvent from the cleft. Also, the DNA–protein contacts are shown to be closest around the 3′ terminus of the primer strand. These observations together suggest that the DNA binding cleft is narrowest around the primer 3′ terminus and that the cleft is wider in the region that contacts the upstream portion of the DNA.

These conclusions are based on the parameters reported in Tables I and III, which are obtained with the assumption of a homogeneous probe population. However, it is shown later that the DNA–protein complex actually exists in two forms. The parameters in Tables I and III therefore represent an average of the two probe populations that arise from the two binding modes of the DNA–protein complex. It is shown later that the polymerase mode of the complex has an abundance of 88%. The parameters in Tables I and III are therefore mostly representative of the polymerase mode of the complex, and the fluorescence footprint defines the region of the DNA primer strand that contacts the protein when the primer 3′ terminus is bound in the polymerase active site.

The DNA–Protein Complex Exists in Two Forms. The fluorescence anisotropy decay measured with the dansyl probe at position +7 in the DNA–protein complex exhibits a curious "dip and rise" (Figure 6A). Anisotropy decay curves that display a high initial value and that rise at long times are due to a heterogeneous fluorophore population (Ludescher et al., 1987). This behavior arises when the fluorophores are distributed between at least two environments and the fluorescence decay and rotational dynamics of the fluorophore are different in each environment.

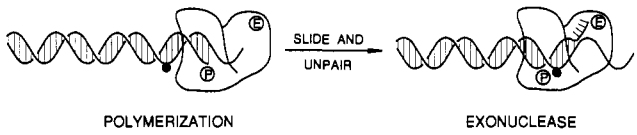

FIGURE 7: Proposed binding modes of the DNA–protein complex. The black circles denote the fluorescent probe in the dansyl-labeled 17*/20-mer. The probe is solvent-exposed in the polymerization mode shown on the left and is buried in the exonuclease mode shown on the right. The active sites for the polymerization reaction and the 3′→5′ exonuclease reaction are denoted P and E, respectively. The DNA and protein are not shown to scale.

The fluorescence footprinting results imply that the major population of dansyl probes at position +7 in the complex are exposed to the aqueous solvent and not in contact with the protein. The existence of the "dip and rise" in the anisotropy curve, however, implies that a minor population of dansyl probes have a longer fluorescence lifetime and a slower, or more restricted, internal rotation than the exposed probes. Since these properties are characteristic of buried dansyl probes, the minor population could arise from a second binding mode of the DNA–protein complex in which position +7 is in contact with the protein. The existence of two binding modes of the DNA–protein complex could correlate with the two distinct activities of the Klenow fragment, since the active sites for the polymerization and 3′→5′ exonuclease reactions are located on different domains of the protein (Freemont et al., 1986; Derbyshire et al., 1988). Studies performed with a biotinylated oligonucleotide duplex suggest that the positions of the primer 3′ terminus during the polymerization and 3′→5′ exonuclease reactions differ by a distance of about 30 Å (Cowart et al. 1989).

The model proposed by Joyce and Steitz for the binding of the DNA primer terminus in the 3′→5′ exonuclease active site can account for the two probe populations responsible for the "dip and rise" in the anisotropy decay (Figure 7). According to this model, the DNA–protein complex has two distinct binding modes. In the major form of the complex, the DNA duplex is bound with the primer 3′ terminus at the polymerase active site (Figure 7). The substrate position +7 is then exposed to the solvent, as shown by the fluorescence footprinting data. The dansyl probe is solvent-exposed in this binding mode and consequently has a short fluorescence lifetime and rotates internally through a large angular range. In the minor form of the DNA–protein complex, the protein has translocated about eight bases upstream on the DNA, and the primer 3′ terminus is bound at the 3′→5′ exonuclease active site (Figure 7). The substrate position +7 is then predicted to lie within the protein structure. The dansyl probe is buried in this binding mode and consequently has a long fluorescence lifetime and its internal rotation is sterically restricted by the DNA–protein contacts. The two binding modes of the DNA–protein complex therefore give rise to a mixture of solvent-exposed and buried dansyl probes. The solvent-exposed probe population dominates the fluorescence at early times after excitation, since the polymerase mode is the major form of the DNA–protein complex. The fluorescence anisotropy thus initially decays to a low value, by virtue of the large-amplitude internal rotation of the solvent-exposed dansyl probes. However, the buried probe population dominates the fluorescence at later times, since their fluorescence is longer lived than that of the exposed probes. Therefore, at later times in the decay, the fluorescence anisotropy rises to a value characteristic of the restricted motion of the buried probes. This model of buried and exposed dansyl probes therefore produces a "dip and rise" in the anisotropy decay.

The "dip and rise" in the anisotropy decay is only observed when the probe is at substrate position +7. However, the distribution of the two binding modes of the DNA–protein complex should be independent of the probe position, and the question arises as to why the phenomenon is not observed with all the DNA–protein complexes. When the probe is at position +7, it is solvent-exposed in the major form of the DNA–protein complex and is buried in the minor form of the complex. The probe heterogeneity resulting from the two binding modes is greatest in this case and leads to the distinctive anisotropy decay. However, when the probe is at substrate positions +1, +2, and +4, it is buried in both forms of the DNA–protein complex. Although the local probe environment is probably different in the two forms of the complex in these cases, this difference is not enough to alter the fluorescence lifetimes and internal rotational motion of the probe sufficiently to generate a "dip and rise" in the anisotropy decay. This explains why the anisotropy decay of these complexes can be analyzed with the assumption of a homogeneous probe population, as reported in Table III.

The "dip and rise" in the anisotropy decay could potentially arise for different reasons than considered above: (i) Incomplete extension of the 11*-mer primer oligonucleotide to the 17*-mer would generate a subset of shorter primers in which the dansyl probe is closer to the 3′ terminus. A mixture of exposed and buried probes will then result, even if the DNA is bound exclusively in the polymerase site. However, elongation of the labeled 11*-mer oligonucleotide is complete under the conditions used here (Allen & Benkovic, 1989). (ii) Degradation of the 17*/20-mer DNA by the 3′→5′ exonuclease activity of the Klenow fragment would generate a subset of shortened primers, and hence a mixture of exposed and buried probes as noted above. However, exonucleolytic degradation of the DNA is prevented by the presence of a large pool of dNTP's, and the primer strand length is constant throughout the fluorescence decay measurement, as described earlier. (iii) Excitation of a higher energy excited state of the dansyl probe, combined with anisotropic rotational diffusion of the probe at position +7, could produce a rising portion in the anisotropy decay (Ludescher et al., 1987). However, the anisotropy decay of the 17*/20/KF complex is the same when excitation wavelengths between 310 and 328 nm are used, even though the contribution of higher energy state to the excitation is varying within this range (Figure 3). (iv) Solvent relaxation around the exposed dansyl probe could rotate the emission dipole and influence the anisotropy decay, although it is not clear that this mechanism would produce a "dip and rise" in the decay. The anisotropy decay would depend on the emission wavelength in this case, but no dependence is seen with the 17*/20/KF complex.

The model shown in Figure 7, whereby the "dip and rise" in the anisotropy decay is correlated with the two binding modes of the complex, is consistent with the experimental data. The uniqueness of the model was established in two ways. First, the 17*/20-mer DNA was modified in such a way as to perturb the distribution of binding modes in favor of the polymerization mode, and the effect on the probe's anisotropy decay was then determined. This was done by incorporating an epoxy-AMP residue at the 3′ terminus of the primer strand of the 17*/20-mer (Figure 2). Epoxy-AMP is an analogue of dAMP containing an epoxide ring across the 2′- and 3′-carbons of the ribofuranose ring. After the incorporation of epoxy-AMP at the primer 3′ terminus, the DNA is bound very tightly in the polymerase site, and translocation to the exonuclease site is hindered (Catalano & Benkovic, 1989).

The modified complex 17*(e)/20/KF was prepared by elongating the 11*-mer with dGTP, dCTP, and epoxy-ATP according to the template sequence shown in Figure 2. The resulting primer oligonucleotide is then terminated with epoxy-AMP, and the dansyl probe is located seven bases upstream, as before. However, the anisotropy decay of this complex does not exhibit a pronounced "dip and rise". Further, the decay time ϕ_2 obtained with the assumption of a homogeneous probe population is close to the value expected for tumbling of the complex (Table III) and is therefore not anomalously large as seen before with heterogeneous probe populations. The heterogeneity of the probe population in this complex is indeed reduced compared with the corresponding complex formed with unmodified 17*/20-mer DNA, as expected if the epoxy-terminated DNA is bound mainly at the polymerase site. The analysis of the anisotropy decay in terms of a mixture of exposed and buried probes (eq 8) confirms this conclusion, since x_b is reduced by a factor of 3 compared with the unmodified 17*/20-mer. The anisotropy decay therefore reflects the expected shift in the distribution of binding modes of the complex resulting from epoxy modification of the primer strand. Further, this result eliminates the possibility that the "dip and rise" can occur even when the DNA is bound exclusively in the polymerase site, for example, due to two different configurations of the propyl chain linker, one of which places the probe in solution while the other brings the probe into contact with the protein. Additionally, this result rules out the possibility that the flexible region of the polypeptide chain between residues 569 and 626, which is disordered in the crystal structure of the Klenow fragment (Ollis et al., 1985), may adopt two configurations in the complex, one of which brings it into contact with the dansyl probe at position +7 when the DNA is bound exclusively at the polymerase site. In a control experiment using dATP in place of epoxy-ATP, the "dip and rise" in the anisotropy decay is present, and ϕ_2 is again found to be anomalously large when the decay is analyzed in terms of a homogeneous probe population (Table III). The absence of the "dip and rise" in the 17*(e)/20′/KF complex is therefore specifically due to the epoxy-AMP residue at the primer terminus and not to the different base sequence of the primer and template oligonucleotides.

The second method of verifying the model shown in Figure 7 was to perturb the DNA binding at the 3′→5′ exonuclease site by modifying the Klenow fragment by site directed mutagenesis. The double mutant D355A, E357A has normal polymerase activity and was used to elongate the labeled 11*-mer primer oligonucleotide. This mutant protein lacks 3′→5′ exonuclease activity and does not bind deoxynucleoside monophosphates, which bind to the exonuclease domain of the wild-type Klenow fragment (Derbyshire et al., 1988). The crystal structure of the mutant protein has been determined and is essentially identical with the structure of the wild-type Klenow fragment except for the two modified amino acids and the absence of two divalent metal ions from the exonuclease domain (Derbyshire et al., 1988). One of the metal ions appears to have a structural role, necessary for the binding of DNA to the exonuclease domain, while the other appears to catalyze the exonuclease reaction (Derbyshire et al., 1988). The mutant protein will therefore bind duplex DNA normally in the polymerase domain, but the DNA binding in the exonuclease domain should be perturbed. The complex of 17*/20-mer DNA with the D355A, E357A mutant Klenow fragment does not exhibit the "dip and rise" in the anisotropy decay (Figure 6B). The anisotropy decay can be analyzed as a homogeneous probe population, and the decay time ϕ_2 is close to the expected tumbling time of the complex. The dansyl probe is therefore predominantly localized in a single environment in this complex. This is confirmed by the analysis according to eq 8, in which the fraction of buried dansyl probes is found to be much smaller than in the corresponding complex obtained with the wild-type protein. The mutations in the exonuclease domain and the consequent loss of both metal ions thus appear to reduce the abundance of the editing mode of the complex to a level where it no longer produces an obvious "dip and rise" in the anisotropy decay of the probe. Since the only structural change in the mutant protein is in the region of the exonuclease site (Derbyshire et al., 1988), and this change is found to reduce the abundance of the minor form of the DNA–protein complex, it is reasonable to conclude that the minor form is indeed associated with DNA bound at the exonuclease site, rather than a nonproductive mode of binding in which the primer 3′ terminus is not bound in either active site. The mutant polymerase may still be able to slide on the DNA, but the residence time of the primer terminus at the 3′→5′ exonuclease site is apparently reduced to the point where the equilibrium population of this binding mode is very small.

The data presented here demonstrate the validity of the model of two distinct binding modes of the complex that arise from DNA binding in either the polymerase or the 3′→5′ exonuclease active sites (Figure 7). However, they do not provide any information on the time scale of interconversion of the two binding modes, except that it is slow on the fluorescence time scale (slower than 100 ns), and they cannot discriminate between different mechanisms of interconversion. The interconversion may occur by a sliding mechanism (intramolecular transfer), as proposed by Joyce and Steitz (1987), or by dissociation of the DNA from one active site and rebinding at the other active site (intermolecular transfer). The Klenow fragment appears to use both pathways during editing (Joyce, 1989).

Abundance of the Two Binding Modes. The precise form of the "dip and rise" in the anisotropy decay curve depends on the relative number of exposed and buried probes, and hence the abundance of each binding mode of the DNA–protein complex. Equation 8 was used to represent the anisotropy decay of a mixture of exposed and buried dansyl probes. The "dip and rise" in the anisotropy decay of the 17*/20/KF complex could be reproduced with this equation by adjusting the mole fraction of buried dansyl probes, which gave $x_b = 0.12 \pm 0.015$. The abundance of the exonuclease mode of the 17*/20/KF complex is therefore estimated to be 12%. This is reasonable since all the base pairs in the 17*/20-mer duplex are matched and the DNA should reside mostly in the polymerase active site under these conditions.

This estimate assumes that all the buried probes arise from the exonuclease mode of the DNA–protein complex. However, if the protein is sliding along the DNA, then it can be bound at positions that are intermediate between those shown in Figure 7. Since the dansyl probe could be buried in some of these intermediate configurations, x_b actually represents an upper limit for the abundance of the exonuclease mode of the DNA–protein complex. However, if the sliding is fast compared with the residence time of the primer terminus at each active site, then the equilibrium population of these intermediate configurations will be negligible. This situation probably applies to the Klenow fragment since the rates of the polymerization and 3′→5′ exonuclease reactions are much smaller than the estimated translocation rate (Kuchta et al., 1987, 1988).

The effect of chemical modification of the DNA or site-directed mutagenesis of the protein on the abundance of the two binding modes of the DNA–protein complex was also analyzed by using eq 8. The epoxy modification of the DNA primer terminus reduced the abundance of the exonuclease mode from 12% to 4%. This modification does indeed shift the distribution of binding modes in favor of the polymerization mode, as expected (Catalano & Benkovic, 1989). In the case of the D355A, E357A mutant protein, the abundance of the exonuclease mode is reduced to 3%. This result implies that the binding of the 17*/20-mer DNA to the exonuclease site of the mutant protein is not completely abolished but it is significantly reduced compared to the wild-type protein. The mutant protein does not bind either of the two divalent metal ions, designated A and B, which are normally bound in the exonuclease active site (Derbyshire et al., 1988). In a cocrystal of dTMP with Klenow fragment, metal ion A is coordinated by the carboxylate groups of Asp355, Glu357, and Asp501 and the phosphate of dTMP (Ollis et al., 1985). The latter interaction presumably occurs with the terminal phosphate group in the DNA primer strand bound at the exonuclease site. The reduced binding of the 17*/20-mer to the exonuclease site of the mutant protein is consistent with the possibility that metal ion A contributes to DNA binding at this site, although the loss of the other metal ion may also contribute to the effect.

It is apparent that the form of the anisotropy decay is very sensitive to the abundance of each binding mode of the DNA–protein complex, even to the presence of very small amounts of the exonuclease mode. This method can therefore be used to study the distribution of the two binding modes under a variety of conditions in solution. In particular, the molecular basis of the editing mechanism can be investigated. The model shown in Figure 7 predicts that the presence of a mismatched nucleotide at the 3′ terminus of the primer strand will increase the abundance of the exonuclease mode of the complex, and hence increasing the editing efficiency, since it will destabilize the double helix and promote local melting of the primer terminus. The molecular properties of the DNA and protein that determine how the separate polymerization and editing activities are coordinated can be investigated by using the method developed here to measure the distribution of binding modes of the DNA–protein complexes formed with a variety of dansyl-labeled DNA oligomers and mutant proteins.

Conclusions

Fluorescence anisotropy decay of site specifically labeled DNA substrates appears to be a very sensitive technique for detecting heterogeneous binding to a protein. The presence of a minor bound form can be readily detected at long times in the decay if the probe has a longer fluorescence lifetime and a more rigid environment than that of the major form. This is because the longest lived fluorophores dominate the fluorescence at sufficiently long times in the fluorescence decay, even though they may represent a small fraction of the total ground-state fluorophore population.

We have been able to map the specific region of contact between the Klenow fragment and DNA and to obtain some information on the DNA–protein interactions within that region. Further, we have shown that duplex DNA molecule bound to the Klenow fragment in solution is distributed between the polymerase and the 3′→5′ exonuclease active sites. In the absence of mismatched bases in the DNA, the DNA resides mostly (88%) in the polymerase active site. The distribution of the two distinct binding modes of the DNA–protein complex can be investigated under a variety of conditions by the present approach since the form of the anisotropy decay is very sensitive to the fraction of labeled DNA bound at each active site.

Acknowledgments

We thank Brian Eger for assistance with some of the experiments reported here.

References

Allen, D. J., & Benkovic, S. J. (1989) *Biochemistry 28*, 9586–9593.

Allen, D. J., Darke, P. L., & Benkovic, S. J. (1989) *Biochemistry 28*, 4601–4607.

Bevington, P. R. (1969) *Data Reduction and Error Analysis for the Physical Sciences*, McGraw-Hill, New York.

Brutlag, D., & Kornberg, A. (1972) *J. Biol. Chem. 247*, 241–248.

Brutlag, D., Atkinson, M. R., Setlow, P., & Kornberg, A. (1969) *Biochem. Biophys. Res. Commun. 37*, 982–989.

Catalano, C. E., & Benkovic, S. J. (1989) *Biochemistry 28*, 4374–4382.

Chen, R. F. (1967) *Arch. Biochem. Biophys. 120*, 609–620.

Chen, R. F., & Scott, C. H. (1985) *Anal. Lett. 18 (A4)*, 393–421.

Cowart, M., Gibson, K. J., Allen, D. J., & Benkovic, S. J. (1989) *Biochemistry 28*, 1975–1983.

Cross, A. J., & Fleming, G. R. (1984) *Biophys. J. 46*, 45–56.

Dale, R. M. K., Livingston, D. C., & Ward, D. C. (1973) *Proc. Natl. Acad. Sci. U.S.A. 70*, 2238–2242.

Derbyshire, V., Freemont, P. S., Sanderson, M. R., Beese, L., Friedman, J. M., Joyce, C. M., & Steitz, T. A. (1988) *Science 240*, 199–201.

Freemont, P. S., Friedman, J. M., Beese, L. S., Sanderson, M. R., & Steitz, T. A. (1988) *Proc. Natl. Acad. Sci. U.S.A. 85*, 8924–8928.

Jovin, T. M., Englund, P. T., & Bertsch, L. L. (1969) *J. Biol. Chem. 244*, 2996–3008.

Joyce, C. M. (1989) *J. Biol. Chem. 264*, 10858–10866.

Joyce, C. M., & Steitz, T. A. (1987) *Trends Biochem. Sci. (Pers. Ed.) 12*, 288–292.

Joyce, C. M., Fujii, D. M., Laks, H. S., Hughes, C. M., & Grindley, N. D. F. (1985) *J. Mol. Biol. 186*, 283–293.

Kinosita, K., Kawato, S., & Ikegami, A. (1977) *Biophys. J. 20*, 289–305.

Kornberg, A. (1980) in *DNA Replication*, W. H. Freeman, San Francisco.

Kuchta, R. D., Mizrahi, V., Benkovic, P. A., Johnson, K. A., & Benkovic, S. J. (1987) *Biochemistry 26*, 8410–8417.

Kuchta, R. D., Benkovic, P., & Benkovic, S. (1988) *Biochemistry 27*, 6716–6725.

Lambooy, P. K., Steiner, R. F., & Sternberg, H. (1982) *Arch. Biochem. Biophys. 217*, 517–528.

Lipari, G., & Szabo, A. (1980) *Biophys. J. 30*, 489–506.

Ludescher, R. D., Peting, L., Hudson, S., & Hudson, B. (1987) *Biophys. Chem. 28*, 59–75.

Millar, D. P., Allen, D. J., & Benkovic, S. J. (1990) *Proc. SPIE—Int. Soc. Opt. Eng. 1204*, 392–403.

Mizrahi, V., Benkovic, P., & Benkovic, S. J. (1986) *Proc. Natl. Acad. Sci. U.S.A. 83*, 5769–5773.

Ollis, D. L., Brick, P., Hamlin, R., Xuong, N. G., & Steitz, T. A. (1985) *Nature 313*, 762–766.

Ondera, M., Shiokawa, H., & Takagi, T. (1976) *J. Biochem. 79*, 195–201.

Steitz, T. A. (1990) *Q. Rev. Biophys. 23*, 205–280.

Warwicker, J., Ollis, D., Richards, F. M., & Steitz, T. A. (1985) *J. Mol. Biol. 186*, 645–649.